THE ASTROPHYSICAL JOURNAL, 549:1062–1075, 2001 March 10

THE DOMINANCE OF DYNAMIC BARLIKE INSTABILITIES IN THE EVOLUTION OF A MASSIVE STELLAR CORE COLLAPSE THAT "FIZZLES"

JAMES N. IMAMURA
Institute of Theoretical Science and Department of Physics, University of Oregon, Eugene, OR 97403

AND

RICHARD H. DURISEN
Department of Astronomy, Indiana University, Bloomington, IN 47405
Received 2000 July 16; accepted 2000 October 24

ABSTRACT

Core collapse in a massive rotating star may halt at subnuclear density if the core contains angular momentum $J \gtrsim 10^{49}$ g cm^2 s^{-1}. An aborted collapse can lead to the formation of a rapidly rotating equilibrium object, which, because of its high electron fraction, $Y_e > 0.4$, and high entropy per baryon, $S_b/k \approx 1$–2, is secularly and dynamically stable. The further evolution of such a "fizzler" is driven by deleptonization and cooling of the hot, dense material. These processes cause the fizzler both to contract toward neutron star densities and to spin up, driving it toward instability points of the barlike modes. Using linear stability analyses to study the latter case, we find that the stability properties of fizzlers are similar to those of Maclaurin spheroids and polytropes despite the nonpolytropic nature and extreme compressibility of the fizzler equation of state. For fizzlers with the specific angular momentum distribution of the Maclaurin spheroids, secular and dynamic barlike instabilities set in at $T/|W| \approx 0.14$ and 0.27, respectively, where T is the rotational kinetic energy and W is the gravitational energy of the fizzler, the same limits as found for Maclaurin spheroids. For fizzlers in which angular momentum is more concentrated toward the equator, the secular stability limits drop dramatically. For the most extreme angular momentum distribution we consider, the secular stability limit for the barlike modes falls to $T/|W| \approx 0.038$, compared with $T/|W| \approx 0.09$–0.10 for the most extreme polytropic cases known previously (Imamura et al.). For fixed equation-of-state parameters, the secular and dynamic stability limits occur at roughly constant mass over the range of typical fizzler central densities. Deleptonization and cooling decrease the limiting masses on timescales shorter than the growth time for secular instability. Consequently, unless an evolving fizzler reaches neutron star densities first, it will always encounter dynamic barlike instabilities before secular instabilities have time to grow. Quasi-linear analysis shows that the angular momentum loss during the early nonlinear evolution of the dynamic barlike instability is dominated by Newtonian self-interaction gravitational torques rather than by the emission of gravitational wave (GW) radiation. GW emission may dominate after the initial dynamic evolutionary phase ends. Nonlinear hydrodynamics simulations with a proper equation of state will be required to determine the ultimate outcome of such evolutions and to refine predictions of GW production by barlike instabilities.

Subject headings: black hole physics — hydrodynamics — instabilities — stars: rotation — supernovae: general

1. INTRODUCTION

Stable, stationary, degenerate equilibrium configurations are possible only for stars with central density $\rho_c \approx 10^4$–10^9 g cm^{-3} (white dwarfs) and $\rho_c \approx 10^{14}$–10^{15} g cm^{-3} (neutron stars). Nonrotating objects with ρ_c between those of white dwarfs and neutron stars are unstable to radial collapse because of the low effective Γ_1 of their equation of state (EOS) (see Shapiro & Teukolsky 1983). These states can be stabilized against collapse by rapid rotation (Shapiro & Lightman 1976; Tohline 1984). This possibility gives rise to the concept of a *fizzler*, the term coined by Gold (1974) to describe the delayed collapse of material toward neutron star densities by the formation of a rotating state intermediate between white dwarfs and neutron stars. In the mid-1980s, Müller & Eriguchi (1985) numerically investigated the properties of fizzlers using a cold β-equilibrium EOS. They found that the range of densities available for fizzlers was restricted. More recently, Hayashi, Eriguchi, & Hashimoto (1998, 1999) showed that *hot* fizzlers were stable against axisymmetric collapse over a much wider range of densities. Citing stability work by others, Hayashi et al. noted that hot fizzlers are secularly unstable to barlike modes driven by gravitational radiation reaction (GRR) for $T/|W| > 0.14$, where T is the rotational kinetic energy and W is the gravitational potential energy of the object. This leads to the traditional fizzler scenario in which collapse *fizzles* because the relatively slow drain of angular momentum resulting from the GRR-driven secular instability permits a quasi-static approach to neutron star density and thereby avoids a supernova event. Here we propose a modified fizzler scenario. We argue that the initial fizzler that forms during core collapse is neither secularly nor dynamically unstable to barlike modes and so the approach to neutron star densities is driven by deleptonization and cooling of the hot dense material. Deleptonization and cooling cause the fizzler to contract and to spin up, which may drive it to instability. In this paper, we investigate the case in which fizzlers have enough angular momentum to encounter a rotational instability point before reaching neutron star densities. Combining detailed equilibrium model construction and linear analyses with timescale arguments, we find that dynamic instabilities rather than secular

ones play the dominant role in evolving fizzlers and that dynamically unstable fizzlers can readily form from rotating precollapse cores with masses in the expected range, between 1.25 and 2.05 $M_\odot$ according to Timmes, Woosley, & Weaver (1996). Dynamic barlike instabilities may be an unavoidable consequence of core collapse in massive stars with very rapid rotation.

Interest in fizzlers has increased recently because they may be strong sources of gravitational wave (GW) radiation. It was, in fact, first conjectured in the 1970s that collapsing rotating stars could be sources of gravitational radiation. However, during the early 1990s, the consensus was that collapsing rotating stars were not efficient sources of gravitational radiation. Finn & Evans (1990) showed that a collapsing rotating stellar core would radiate only $\sim 10^{-8}$ Mc^2 in gravitational waves and, consequently, would be visible by LIGO only within our Galaxy and the Magellanic Clouds (Abramovici et al. 1995). Several studies have reconsidered this issue. For example, Houser (1998) showed for stiff polytropes with 1.4 $M_\odot$ and $R_{\rm eq} = 15$ km that unstable bar modes could produce time-integrated GW luminosities as large as 10^{-3} Mc^2. The GW luminosity and the waveform are uncertain, however, because it is difficult to determine the long-term outcome of barlike instabilities using hydrodynamics simulations (Pickett, Durisen, & Davis 1996; Smith, Houser, & Centrella 1996; Houser 1998; Imamura, Durisen & Pickett 2000; New, Centrella, & Tohline 2000; Shibata, Baumgarte, & Shapiro 2000; Durisen et al. 2000). Given the potential importance of fizzlers to the next generation of gravitational wave detectors, further research is needed. This paper presents results on the secular and dynamic barlike instabilities of hot fizzlers. The linear tools of Toman et al. (1998) are used to determine stability limits, eigenfunctions, eigenfrequencies, and growth times, while the quasi-linear technique developed by Imamura et al. (2000) is used to characterize the early nonlinear evolution of the dynamic instabilities, including an assessment of gravitational wave production. In a future paper, we will consider long-term fizzler evolution using nonlinear hydrodynamic simulations and compute the gravitational radiation produced by unstable fizzlers.

The remainder of this paper is organized as follows. The mathematical models and methods are described in § 2. The numerical results are presented in § 3. Discussions of fizzler evolution and the gravitational wave luminosity of evolving fizzlers are presented in § 4. Our results are summarized in § 5.

2. MATHEMATICAL MODELS

2.1. *Equilibrium Configurations*

The equation of motion in steady state is

$$(\boldsymbol{v}\cdot\nabla)\boldsymbol{v} + \frac{1}{\rho}\nabla P + \nabla\Phi_g = 0\ , \tag{1}$$

where P is the pressure, v is the velocity, and Φ_g is the gravitational potential. The equation of state (EOS) of the hot, dense stellar material is nonpolytropic; however, following Hayashi et al. (1998), we assume that it is barotropic. This eliminates the need for solution of the energy equation and requires that the object rotate on cylinders (see Tassoul 1978), in other words, $v_\phi = \Omega(\varpi)\varpi\hat{\boldsymbol{\phi}}$ and $v_\varpi = v_z = 0$, where (ϖ, ϕ, z) are cylindrical coordinates about the rotation axis, the z-axis. To define the pressure, we use the EOS of Lattimer & Swesty (1991), which is based on the compressible liquid drop model of nuclei. For a given nuclear compressibility K, electron fraction Y_e, and entropy per baryon S_b, the pressure and temperature are functions of the baryon number density alone. Using ρ and P for given K, Y_e, and S_b, we define a barotropic EOS, which we approximate by a series of piecewise polytropic functions, $P(\rho) = K_i(\rho)\rho^{1+1/n_i(\rho)}$ (Müller & Eriguchi 1985). The quantities $K_i(\rho)$ and $n_i(\rho)$ are defined on a grid with spacing $\log(\rho_{i+1}/\rho_i) = 0.02$. Given the piecewise polytropic approximation, the equation of motion can be integrated to yield

$$[n_i(\rho)+1]K_i(\rho)\rho^{1/n_i(\rho)} = C_i(\rho) - \Phi_g - \Phi_c\ , \tag{2}$$

where $C_i(\rho)$ is a ρ-dependent integration constant (Eriguchi & Müller 1991) and Φ_c, the centrifugal potential, is given by

$$\Phi_c(\varpi) = -\int_0^\varpi \Omega^2(\varpi)\varpi\, d^3x\ . \tag{3}$$

To determine $\Omega(\varpi)$, and hence Φ_c, we specify the specific angular momentum distribution $h(m_c)$, where m_c is the mass contained within a cylindrical volume of radius ϖ. Our choices for $h(m_c)$ are defined as follows. The structure of a static polytrope with index n' is calculated. The polytrope is then imagined to rotate uniformly but remain spherical. Uniformly rotating, spherical polytropes define a family of $h(m_c)$ functions parameterized by n' (Bodenheimer & Ostriker 1973). The $n' = 0$ $h(m_c)$ is that of a Maclaurin spheroid. The $h(m_c)$ distributions peak more strongly toward the equatorial radius of the object for larger n'.

We solve for a unique equilibrium object as follows: (1) n' and the EOS parameters are specified. (2) The central density, ρ_c, and the ratio of the polar and equatorial radii, $R_p/R_{\rm eq}$, are set. (3) A $\rho(r)$ distribution and $R_{\rm eq}$ are guessed. (4) Φ_g and Φ_c are calculated using $\rho(r)$ and $h(m_c)$. (5) Equation (2) is solved for $\rho(r)$. (6) The initial $\rho(r)$ and the new $\rho(r)$ are compared. If they are consistent to within some predetermined tolerance, the calculation is declared to have converged. If the $\rho(r)$ distributions are not consistent, new guesses for $\rho(r)$ and $R_{\rm eq}$ are made and steps (4)–(6) repeated. The calculation determines M, $R_{\rm eq}$, and J for the given ρ_c and $R_p/R_{\rm eq}$. The code for this iterative procedure is based on a version of Hachisu's (1986) self-consistent field code.

2.2. *Stability Analyses*

We consider secular and dynamic nonaxisymmetric instabilities in modes that are analogs of the Kelvin modes of incompressible fluids (see Chandrasekhar 1969). The modes have azimuthal dependence $\exp(\pm im\phi)$, where m is a constant and ϕ is the azimuthal angle. Secular instabilities set in when more than one equilibrium configuration exists for a given angular momentum J. One equilibrium state can evolve to another if the second state has lower total energy and an appropriate dissipation mechanism exists. Secular instabilities grow on the dissipation timescale, which is generally much longer than the dynamic timescale for the configuration. Dynamic instabilities occur when small perturbations about equilibrium grow spontaneously on a dynamic timescale.

2.2.1. *Secular Instability*

Secular instability may be driven by gravitational radiation reaction (GRR) or viscous dissipation. Here we consider GRR-driven modes. Secular instabilities driven by GRR set in along sequences of equilibrium rotating models at neutral points where the canonical energy E_c passes

through zero (Friedman & Schutz 1978). We locate neutral points using the Lagrangian variational principle developed by Friedman & Schutz (1978). The canonical energy is

$$E_c = 0.5\omega^2 \int \rho \boldsymbol{\xi}^* \cdot \boldsymbol{\xi}\, d^3x + 0.5 \times \int \boldsymbol{\xi}^* \cdot [\boldsymbol{T}(\boldsymbol{\xi}) + \boldsymbol{V}(\boldsymbol{\xi}) + \boldsymbol{P}(\boldsymbol{\xi})] d^3x\,, \quad (4)$$

where ω is the oscillation frequency of a mode, $\boldsymbol{\xi}$ is the Lagrangian displacement of the perturbation, and

$$\boldsymbol{T}(\boldsymbol{\xi}) = \rho(\boldsymbol{v}\cdot\boldsymbol{V})^2\boldsymbol{\xi} - \rho(\boldsymbol{\xi}\cdot\boldsymbol{V})(\boldsymbol{v}\cdot\boldsymbol{\nabla})\boldsymbol{v}\,, \quad (5)$$

$$\boldsymbol{V}(\boldsymbol{\xi}) = -\rho\boldsymbol{\nabla}\delta\Phi\,, \quad (6)$$

$$\boldsymbol{P}(\boldsymbol{\xi}) = \left(\frac{\boldsymbol{\nabla}P}{\rho}\right)(\boldsymbol{\nabla}\boldsymbol{\nabla}\cdot\rho\boldsymbol{\xi}) - \boldsymbol{\nabla}(\Gamma P\cdot\xi) - \boldsymbol{\nabla}(\boldsymbol{\xi}\cdot\boldsymbol{\nabla}P) \quad (7)$$

(Clement 1979). To find neutral points ($\omega = 0$) in an inertial frame, we look for places along a sequence of models where the rightmost integral in equation (4) changes sign.

We use the prescription for $\boldsymbol{\xi}$ given in Bardeen et al. (1977, hereafter BFSS),

$$\boldsymbol{\xi} = (A(\varpi),\, i[A(\varpi) + B(\varpi)],\, 0)\varpi^{m-1}\exp(im\phi)\,, \quad (8)$$

where $A(\varpi)$ and $B(\varpi)$ are arbitrary functions. The $\boldsymbol{\xi}$ are constrained only by the requirement that the perturbation conserve circulation on a constant entropy surface. Because of this, we are free to choose either $A(\varpi)$ or $B(\varpi)$ arbitrarily. We let

$$A(\varpi) = \sum_{j=1}^{N} c_j \varpi^{j-1}\,, \quad (9)$$

where the c_j are arbitrary constants and $N = 7$. We find the best c_j (and hence best $\boldsymbol{\xi}$) through minimization of $E_c(\omega = 0)$ with respect to the c_j (Imamura et al. 1995).

2.2.2. *Dynamic Instability*

The properties of dynamic instabilities are found by solving an initial-value problem (IVP) for the evolution away from equilibrium of linearized perturbations of the form

$$\rho = \rho_o + \rho_1\exp(im\phi), \qquad P = P_o + P_1\exp(im\phi)\,, \quad \text{and} \quad v_j = v_{j,o} + v_{j,1}\exp(im\phi) \quad (10)$$

(Toman et al. 1998). Here ρ_1, P_1, and $v_{j,1}$ are the perturbed density, pressure, and velocities, respectively; j denotes ϖ, ϕ, and z; and ρ_0, P_0, and $v_{j,0}$ are the equilibrium density, pressure, and velocity, respectively. The perturbations depend implicitly on time, and the linearized equations form a set of partial differential equations that describes the time evolution of the perturbations about equilibrium. The perturbation equations are complex and solved by converting each complex equation into a pair of real equations. The evolution equations are given in the Appendix. We impose symmetry about the equatorial plane and set P_1, ρ_1, and $v_{j,1}$ to zero on the surface of the fizzler. The continuity of Φ_g at the surface of the fizzler is guaranteed by imposing boundary conditions on the potential on the surface of the cylinder defined by the maximum ϖ and z of the computational grid. The Φ_g on the surface of the cylinder is found by solving the integral form for the perturbed Φ_g.

The equations with the imposed boundary conditions are solved as follows. We use grids of square cells with size $(N_\varpi, N_z) = (128,64)$ in (ϖ, z)-space. The values of ρ_1 and P_1 are defined at cell centers, and those of $v_{j,1}$ at cell vertices. The equations are solved by approximating spatial derivatives with centered finite differences. The system of equations is advanced in time using a Runge-Kutta algorithm. We integrate for more than 20 central initial rotation periods (CIRPs) or until a single exponentially growing global disturbance emerges from imposed random noise. Growth rates are determined by least-squares fits to the exponential growth portion of the evolution, and eigenfrequencies are found by least-squares fits to the linear portions of the phase evolution. The functional forms of ρ_1, P_1, and $v_{j,1}$ are the eigenfunction of the most unstable mode. If exponential growth is not detected after more than 20 CIRPs, the model is deemed dynamically stable to disturbances with the given m-symmetry.

2.3. *Torques*

Barlike modes can redistribute angular momentum through internal Newtonian gravitational torques or through the emission of gravitational wave radiation. We estimate the Newtonian self-interaction torque of the barlike mode using the quasi-linear theory of Imamura et al. (2000). The quasi-linear torque density, integrated over ϕ and z at time t, is

$$\gamma(\varpi) = \pi m\rho_1\Phi_1\sin(\phi_\rho - \phi_\Phi)\,, \quad (11)$$

where ϕ_ρ and ϕ_Φ are the phases of ρ_1 and Φ_1, respectively.

To calculate the GW torque, we use the linear eigenfunctions and the slow motion quadrupole GRR torque formula (see Finn & Evans 1990). For rotation about the z-axis and pure m eigenfunctions, only the torque about the z-axis is nonzero, which, from here on, we refer to as $\dot{J}_{\rm GW}$. $\dot{J}_{\rm GW}$ is given by

$$\dot{J}_{\rm GW} = \frac{2G\omega^5}{5c^5}(\mathscr{I}_o^2 + \mathscr{I}_1^2)\,, \quad (12)$$

where

$$\mathscr{I}_o = \frac{\pi}{2}\int \rho_1\cos(\phi_\rho)\varpi^3 d\varpi\, dz$$

and

$$\mathscr{I}_1 = -\frac{\pi}{2}\int \rho_1\sin(\phi_\rho)\varpi^3\, d\varpi\, dz\,. \quad (13)$$

Calculating $\dot{J}_{\rm GW}$ is straightforward for the dynamic bar modes because the IVP determines the eigenfunction and eigenvalues automatically. However, for the secularly unstable modes, it is not as easy. We cannot determine ρ_1 and ω for secularly unstable bar modes beyond the neutral points using the technique given in § 2.2.1. We instead estimate ω by evaluating the Lagrangian variational principle of Lynden-Bell & Ostriker (1967),

$$i\omega\int \rho\boldsymbol{\xi}^*\cdot[(\boldsymbol{v}\cdot\boldsymbol{\nabla})\boldsymbol{\xi} + \boldsymbol{\Omega}\times\boldsymbol{\xi}]d^3x + E_c = 0\,, \quad (14)$$

for trial functions determined by the BFSS constraint equations using a generalization of the circulation constraint given in Imamura et al. (1995).

3. NUMERICAL RESULTS

3.1. *Equilibrium Sequences*

We set K to 180 MeV, and consider entropy per baryon $S_b = 0.7k$ and $1.5k$. We have explored effects of electron fractions Y_e from 0.15 to 0.4. These Y_e and S_b ranges are

roughly those expected for collapsing stellar cores (see Strobel, Schaab, & Weigel 2000). The rest of this paper focuses on $Y_e \leq 0.3$ because secular and dynamic barlike instabilities occur only for plausible fizzler masses ($\leq 2\,M_\odot$) at the lower range of Y_e-values. In Figure 1 we show the effective polytropic index

$$n_{\rm eff} = \left(\frac{\rho}{P}\frac{\partial P}{\partial \rho} - 1\right)^{-1} \tag{15}$$

for $Y_e = 0.2$ and 0.3 and $S_b = 1.5k$ EOSs. In terms of $n_{\rm eff}$, the $Y_e = 0.2$ EOS is somewhat stiffer at most ρ but is still very compressible. It is interesting to note that $n_{\rm eff}$ is slightly less than 3 for the $Y_e = 0.2$ EOS for densities between 10^9 and a few times 10^{12} g cm^{-3}. This makes the effective $\Gamma = 1 + 1/n_{\rm eff}$ slightly greater than 4/3; and so, for $Y_e \lesssim 0.2$, fizzlers in some density ranges are stable against axisymmetric collapse even when they are not rotating. However, such states would not be long-lived because of the effects of electron captures and cooling. On the other hand, fizzlers with $Y_e \gtrsim 0.3$ EOSs have $n_{\rm eff} > 3$ and effective $\Gamma < 4/3$, and so are unstable to radial collapse in the absence of rotation. The Lattimer & Swesty EOS is uncertain for low temperature and for $\rho_c \lesssim 10^7$–10^8 g cm^{-3}. Beyond nuclear density ($\rho_{\rm nuc} \approx 2 \times 10^{14}$ g cm^{-3}), the LS EOS stiffens to $n_{\rm eff} \lesssim 1$.

Structure properties for representative fizzler models are given in Tables 1 and 2. The tables also include eigenvalues for the unstable models. In the next to last column, the oscillation frequencies ω for the unstable barlike modes are given. The ω are found from equation (14) for secular instability or by fitting $m = 2$ Fourier phases in the IVP method for dynamic instability. The pattern period P_p of the $m = 2$ mode is related to ω by $P_p = 4\pi/\omega$. The last column in the tables gives the shorter of the secular and dynamic instability growth times. For secular instabilities, equation (16) from § 3.2 is used. We only give eigenvalues for the secular modes for $T/|W| \lesssim 0.2$ because our method becomes increasingly inaccurate beyond the neutral point, $T/|W| \approx 0.14$ (§ 3.2). For dynamic instability, fits to the exponential growth of dynamically unstable modes in the IVP method are used.

In Figure 2 we show plots of fizzler mass M versus central density ρ_c for $n' = 0$ and for EOSs with $Y_e = 0.2$ and 0.3 and $S_b = 1.5k$ and $0.7k$. Beyond $\rho_c \approx 10^{14}$ g cm^{-3}, our Newtonian approach becomes increasingly inaccurate because effects of general relativity are increasingly important. The solid lines are lines of constant total fizzler angular momentum, $J = 0$, 5×10^{49}, and 2.5×10^{50} g cm^2 s^{-1}. As discussed by Hayashi et al., models along sequences with the same J whose curves in the (M, ρ_c)-plane slope downward are unstable to axisymmetric collapse. For $Y_e \lesssim 0.3$, as illustrated in Figure 2*a*, the curves for nonrotating fizzlers slope downward; but, for $J \gtrsim 10^{49}$ g cm^2 s^{-1}, the models are stable against axisymmetric collapse because they have J-constant curves that slope upward. For nonaxisymmetric perturbations, the dotted lines labeled "sec" and "dyn" mark the onset of the secular and dynamic barlike instabilities, respectively (see § 3.2). For given EOS and $\rho_c < \rho_{\rm nuc}$, the stability limits are lines of roughly constant M. As can be seen by comparing the various panels in Figure 2, these stability limits are lower for smaller Y_e and S_b, depending more strongly on Y_e than on S_b. As explained later in § 4.2, this mass constancy of the stability limits, combined with their decrease in mass as the fizzler deleptonizes (lowering Y_e) and cools (lowering S_b), has profound consequences for fizzler evolution.

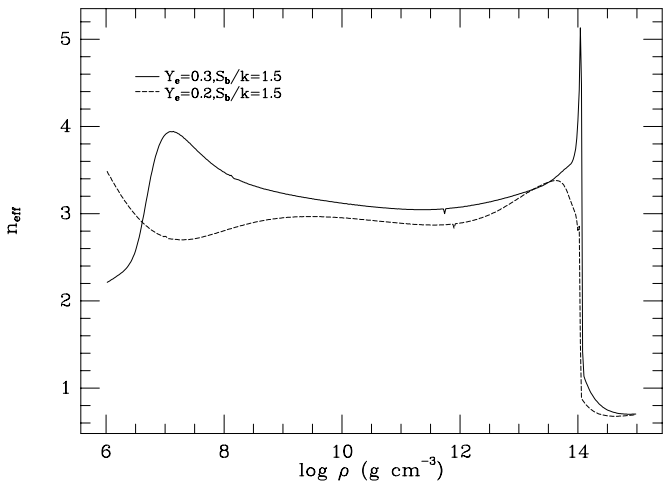

FIG. 1.—Effective polytropic indices for the Lattimer-Swesty EOS. The effective polytropic index, $n_{\rm eff}$, is defined by $\partial P/\partial \rho = (1 + 1/n_{\rm eff})(P/\rho)$. We show $K = 180$ MeV, $Y_e = 0.2$ and $S_b = 1.5k$ (*dashed line*), and $Y_e = 0.3$ and $S_b = 1.5k$ (*solid line*).

In Figure 3 we present $\rho(r)$ structures for $n' = 0$ fizzlers near the secular and dynamic barlike stability limits, $T/|W| \approx 0.14$ and 0.27. We show fizzlers with $Y_e = 0.2$ and $S_b = 1.5k$, and $\rho_c = 10^{12}$, 10^{14}, and 2.51×10^{14} g cm^{-3}. The centers of the $\rho_c = 2.51 \times 10^{14}$ g cm^{-3} models are beyond the transition to the stiff EOS regime. The $T/|W| \approx 0.14$ fizzlers have $M = 0.520$, 0.497, and 1.24 $M_\odot$. The $T/|W| \approx 0.27$ fizzlers have $M = 1.12$, 1.07, and 2.61 $M_\odot$. Other data on the 10^{12} and 10^{14} g cm^{-3} models in Figure 3 are given in Table 2. For $\rho_c < \rho_{\rm nuc}$, the fizzlers are very compressible and, consequently, are strongly centrally condensed and flare as the equatorial radius is approached. For $\rho_c > \rho_{\rm nuc}$, the fizzlers are stiffer and more boxlike in shape. However, where ρ is small, they still flare strongly and thus differ from pure stiff polytropes (see, for instance, Pickett et al. 1996).

Only $Y_e = 0.2$ fizzler models are illustrated in Figure 3 because the $\rho(r)$ structures are qualitatively similar for the range of Y_e we consider. On the other hand, the $\rho(r)$ structures can vary dramatically with n'. Equilibrium properties for $Y_e = 0.3$ and $S_b/k = 1.5$, $n' = 3$ fizzlers are given in Table 3. In Figure 4*a* we show $\rho_c = 10^{14}$ g cm^{-3}, $n' = 3$ fizzlers with $T/|W| = 0.0359$ and 0.132. The $T/|W| = 0.0359$ model is just below the secular stability limit (see § 3.2). The high-$T/|W|$ fizzler has a compact central core and an extensive low-density envelope. To illustrate how radically different fizzlers can be owing to their angular momentum distributions alone, Figure 4*b* shows the $\rho_c = 10^{14}$ g cm^{-3}, $n' = 0$ fizzler with $T/|W| = 0.142$ from Table 1 for the same EOS. Looking at the Table 1 and 3 entries, we see that about 30% more angular momentum is required to support 7% less mass at the same ρ_c when $n' = 3$ rather than zero. The structural differences can be seen by comparing the rightmost panels of Figure 4*a* with Figure 4*b*. The $n' = 3$ model is far more distorted and has much more severe differential rotation.

3.2. *Stability Results*

For $n' = 0$ and $\rho_c = 10^{10}$–10^{14} g cm^{-3}, the neutral points for the GRR-driven modes fall at $T/|W| = 0.13$–0.15, 0.10–0.11, and 0.08–0.09 for $m = 2$, 3, and 4, respectively. The

TABLE 1

EQUILIBRIUM MODELS AND BAR MODE EIGENVALUES: $Y_e = 0.3$, $S_b = 1.5k$, $n' = 0$

$T/\|W\|$	M ($M_\odot$)	J (g cm^2 s^{-1})	CIRP (ms)	R_{eq} (km)	ω (s^{-1})	τ_g (ms)
			$\rho = 10^{12}$ g cm^{-3}			
0.146.....	1.08	2.91×10^{49}	23.9	395	2.8	2.2×10^{15}
0.176.....	1.26	4.32×10^{49}	22.9	440	28	1.3×10^{10}
0.212.....	1.55	7.11×10^{49}	22.3	508	45	1.4×10^{9}
0.257.....	2.11	1.40×10^{50}	22.1	625	...	...
0.270.....	2.34	1.74×10^{50}	22.2	669	...	...
0.284.....	2.62	2.22×10^{50}	22.3	722	148	53.8
0.299.....	3.00	2.92×10^{50}	22.5	788	162	38.0
0.315.....	3.51	4.02×10^{50}	22.8	873	175	29.4
0.323.....	3.81	4.80×10^{50}	23.0	926	181	26.5
			$\rho = 10^{13}$ g cm^{-3}			
0.146.....	1.05	1.90×10^{49}	7.56	182	8.8	1.1×10^{14}
0.176.....	1.22	2.82×10^{49}	7.25	203	86	6.7×10^{8}
0.212.....	1.51	4.64×10^{49}	7.05	234	170	7.0×10^{6}
0.257.....	2.05	9.17×10^{49}	7.00	288	...	...
0.270.....	2.27	1.14×10^{50}	7.02	308	...	...
0.284.....	2.55	1.45×10^{50}	7.05	332	464	17.3
0.299.....	2.92	1.91×10^{50}	7.11	363	507	12.4
0.315.....	3.41	2.62×10^{50}	7.21	402	548	9.56
0.324.....	3.71	3.14×10^{50}	7.26	426	569	8.60
			$\rho = 10^{14}$ g cm^{-3}			
0.142.....	0.953	1.10×10^{49}	2.41	86.0	11	...
0.172.....	1.11	1.63×10^{49}	2.31	95.4	220	9.1×10^{7}
0.208.....	1.37	2.68×10^{49}	2.24	110	470	9.3×10^{5}
0.253.....	1.86	5.29×10^{49}	2.22	135	...	...
0.266.....	2.05	6.56×10^{49}	2.22	144	...	...
0.280.....	2.30	8.36×10^{49}	2.23	155	1,390	6.60
0.295.....	2.63	1.10×10^{50}	2.25	169	1,540	4.51
0.312.....	3.08	1.51×10^{50}	2.28	187	1,670	3.38
0.329.....	3.69	2.21×10^{50}	2.31	211	1,820	2.69

$T/|W|$'s for the neutral points depend only weakly upon ρ_c and EOS. They are, however, very sensitive to $h(m_c)$. For $n' = 3$ fizzlers and $Y_e = 0.2$–0.3, $S_b = 1.5k$, and $\rho_c = 10^{13}$ and 10^{14} g cm^{-3}, the neutral points, drop to $T/|W| = 0.037$–0.038, 0.020–0.021, and 0.013 for $m = 2$, 3, and 4, respectively. This is the same tendency found for polytropes by Imamura et al. (1995). Although there is some concern about the severe distortions in $n' = 3$ models at high $T/|W|$, the left-hand panels of Figure 4*a* indicate that the models have reasonably well-behaved structures for the low $T/|W|$-values near the secular stability limits. So our neutral point location algorithm should be giving accurate results, and the dramatic reduction of the secular stability limit for $n' = 3$ is probably real.

The growth time for the GRR-driven secular instability is

$$\tau_{GRR} \approx \frac{2E_c/\Omega_p}{|\dot{J}_{GW}|} . \tag{16}$$

τ_{GRR} increases strongly with m. If the viscous torque is comparable to or dominates the GRR torque, viscosity increases τ_{GRR} and acts to damp the GRR-driven secular instability (Lindblom & Detweiler 1977). The viscous torque timescale decreases with increasing m, and so high-m GRR-driven modes are easily damped by viscosity (Ipser & Lindblom 1991). Here we therefore use the $m = 2$ mode to define the secular stability limit. For $\rho_c < \rho_{nuc}$, the $n' = 0$ barlike secular stability limits fall at ~ 0.5, 1, and 1.6–1.7 $M_\odot$ for $Y_e = 0.2$, 0.3, and 0.4, respectively. Above ρ_{nuc}, all stability limits rise steeply in M.

The dynamic stability limit for $n' \leq 1.5$ for the barlike modes falls near $T/|W| = 0.27$, similar to the limit found for polytropes (Pickett et al. 1996; Toman et al. 1998). For numerical reasons, we are able to generate models for $n' \gtrsim 2$ with rotation rapid enough to excite the dynamic instability. This is why Table 3 for $n' = 3$ ends with $T/|W| = 0.132$. Dynamic instabilities for $m \geq 3$ modes set in for higher $T/|W|$ than the $m = 2$ barlike mode and are not considered here (see Toman et al. 1998). For fizzlers, the bar mode dynamic stability limit falls at $\sim 2\ M_\odot$ for $Y_e = 0.3$ and $\sim 1\ M_\odot$ for $Y_e = 0.2$ when $\rho_c < \rho_{nuc}$. Above ρ_{nuc}, the M limits increase strongly with ρ_c for all Y_e and S_b.

The flatness and level of the secular and dynamic M-ρ stability curves can be understood analytically. Over the fizzler density range, $\Gamma \approx 4/3$ and so one expects that the mass of a nonrotating fizzler M_{nr} will be approximately constant as a function of ρ. Second, using the virial theorem for $\Gamma = 4/3$ together with approximate homology assumptions, one gets for the fizzler mass

$$M \approx M_{nr}(1 - 2T/|W|)^{-3/2} = M_{nr}\, f . \tag{17}$$

For $T/|W| = 0.14$, $f = 1.637$ and for $T/|W| = 0.27$, $f = 3.205$. For $\rho_c = 10^{10}$ g cm^{-3} in Figure 2*a*, $M_{nr} \approx 0.65\ M_\odot$. Using the values of f above, we estimate $M_{sec} \approx 1.06\ M_\odot$ for the secular stability limiting mass and $M_{dyn} \approx 2.08$

TABLE 2

EQUILIBRIUM MODELS AND BAR MODE EIGENVALUES: $Y_e = 0.2$, $S_b = 1.5k$, $n' = 0$

$T/\|W\|$	M ($M_\odot$)	J (g cm^2 s^{-1})	CIRP (ms)	R_{eq} (km)	ω (s^{-1})	τ_g (ms)
			$\rho = 10^{12}$ g cm^{-3}			
0.148.....	0.520	8.66×10^{48}	23.8	278	5.6	2.6×10^{14}
0.194.....	0.664	1.59×10^{49}	22.5	329	44	3.3×10^{9}
0.222.....	0.788	2.36×10^{49}	22.2	370	63	2.3×10^{8}
0.255.....	0.987	3.86×10^{49}	22.1	432	...	...
0.272.....	1.12	5.11×10^{49}	22.2	479	...	...
0.293.....	1.35	7.45×10^{49}	22.4	533	159	39.8
0.330.....	1.94	1.58×10^{50}	23.1	693	188	23.7
0.340.....	2.18	1.97×10^{50}	23.4	735	195	21.6
			$\rho = 10^{13}$ g cm^{-3}			
0.141.....	0.519	5.72×10^{48}	7.64	129	4.0	...
0.185.....	0.652	1.02×10^{49}	7.19	151	110	4.8×10^{8}
0.222.....	0.811	1.69×10^{49}	7.03	176	200	1.1×10^{7}
0.272.....	1.16	3.71×10^{49}	7.04	226	...	...
0.292.....	1.39	5.34×10^{49}	7.10	253	491	13.3
0.322.....	1.86	9.67×10^{49}	7.26	307	565	8.52
0.330.....	2.01	1.14×10^{50}	7.31	327	584	7.83
			$\rho = 10^{14}$ g cm^{-3}			
0.142.....	0.497	3.69×10^{48}	2.41	63.9	16	...
0.187.....	0.631	6.73×10^{48}	2.27	75.2	340	2.4×10^{7}
0.215.....	0.746	9.94×10^{48}	2.22	84.11	530	1.3×10^{6}
0.248.....	0.931	1.62×10^{49}	2.22	97.6	...	...
0.266.....	1.07	2.20×10^{49}	2.22	107	...	...
0.286.....	1.26	3.13×10^{49}	2.23	120	1,470	5.38
0.318.....	1.71	5.76×10^{49}	2.28	145	1,750	3.04
0.334.....	2.05	8.27×10^{49}	2.32	164	1,890	2.49

$M_\odot$ for the dynamic stability limiting mass, in good agreement with the values in Figure 2*a*. Equation (17), when applied to white dwarfs, also reproduces the secular and dynamic upper mass limits given in Durisen (1977).

In Imamura et al. (2000), we demonstrated that the quasi-linear analysis of § 2.3 does an excellent job of predicting the early nonlinear behavior of dynamically unstable barlike models, including the maximum amplitude attained during nonlinear growth and the fraction of the initial mass contained in the central barlike region. Tables 4 and 5 contain results of applying quasi-linear analyses to the dynamically unstable models from Tables 1 and 2. M_b and J_b are the mass and angular momentum in the central barlike regions, $\dot{J}_b$ is the total Newtonian torque over the bar, and M_d is the mass contained in the spiral arms. The angular momentum transfer (or loss) times $\tau_b = J_b/|\dot{J}_b|$ and $\tau_{GW} = J_b/|\dot{J}_{GW}|$ are calculated for ρ_1 normalized such that

$$\delta\mathcal{M} = \frac{\int |\rho_1| d^3x}{M} = 1 . \tag{18}$$

The τ_b and τ_{GW} scale as $\delta\mathcal{M}^{-2}$. The choice $\delta\mathcal{M} = 1$ gives a good estimate for the minimum expected τ_b and τ_{GW}. The hydrodynamic simulations in Imamura et al. (2000) showed that for $n = 1.5$ and 2.5 polytropes, the amplitude of the dynamic barlike instability peaks at $\delta\mathcal{M} \approx 1$.

TABLE 3

EQUILIBRIUM MODELS: $Y_e = 0.3$, $S_b = 1.5k$, $n' = 3$, FOR $\rho = 10^{14}$ G CM^{-3}

$T/\|W\|$	M ($M_\odot$)	J (g cm^2 s^{-1})	CIRP (ms)	R_{eq} (km)
0.000.....	0.552	0	0	59.1
0.0119.....	0.573	1.26×10^{48}	12.0	73.6
0.0225.....	0.593	1.91×10^{48}	8.75	94.0
0.0359.....	0.622	2.72×10^{48}	6.91	134
0.0454.....	0.643	3.34×10^{48}	6.10	172
0.0600.....	0.679	4.41×10^{48}	5.22	245
0.0712.....	0.710	5.38×10^{48}	4.71	315
0.0883.....	0.760	7.14×10^{48}	4.07	445
0.0964.....	0.784	8.12×10^{48}	3.81	519
0.106.....	0.816	9.48×10^{48}	3.49	626
0.118.....	0.854	1.15×10^{49}	3.06	793
0.132.....	0.891	1.41×10^{49}	2.40	1,068

Two representative barlike structures for $n' = 0$ fizzlers with $Y_e = 0.2$ and $S_b = 1.5k$ are given in Figure 5. We show the real parts of ρ and v in a frame rotating with the bar (eq. [10]), in the equatorial plane. The amplitude of the linear eigenfunction is chosen to satisfy equation (18). If this leads to $\rho < 0$, then ρ is set to 0. The model in Figure 5*a* has $\rho_c = 10^{14}$ g cm^{-3} and $T/|W| = 0.286$, and the one in Figure 5*b* has $\rho_c = 2.51 \times 10^{14}$ g cm^{-3} and $T/|W| = 0.303$. Figure 5 demonstrates how the bar mode structure depends on ρ_c. The $\rho_c < \rho_{nuc}$ fizzler has a compact bar with extensive spiral arms, while the $\rho_c > \rho_{nuc}$ fizzler has a larger bar with weaker spiral arms. For the $\rho_c < \rho_{nuc}$ fizzler, the bar mass $M_b = 0.95\ M_\odot = 0.75M$, the bar angular momentum $J_b = 1.65 \times 10^{49}$ g cm^2 s^{-1} $= 0.53J$, and the bar equatorial radius $R_b = 39$ km $= 0.32\ R_{eq}$. The Newtonian torque $\dot{J}_b = -7.59 \times 10^{50}$ g cm^2 s^{-2}, and the GRR torque

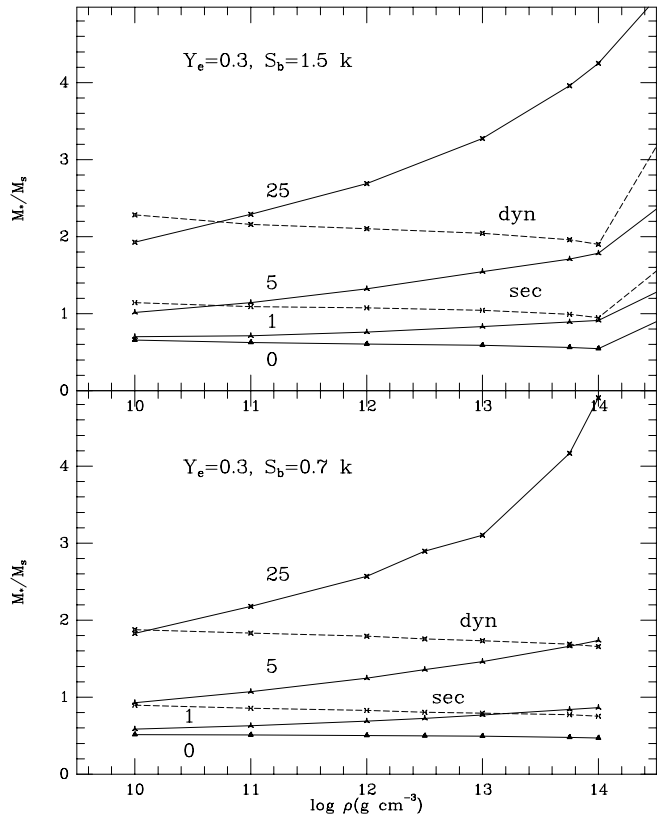

FIG. 2a

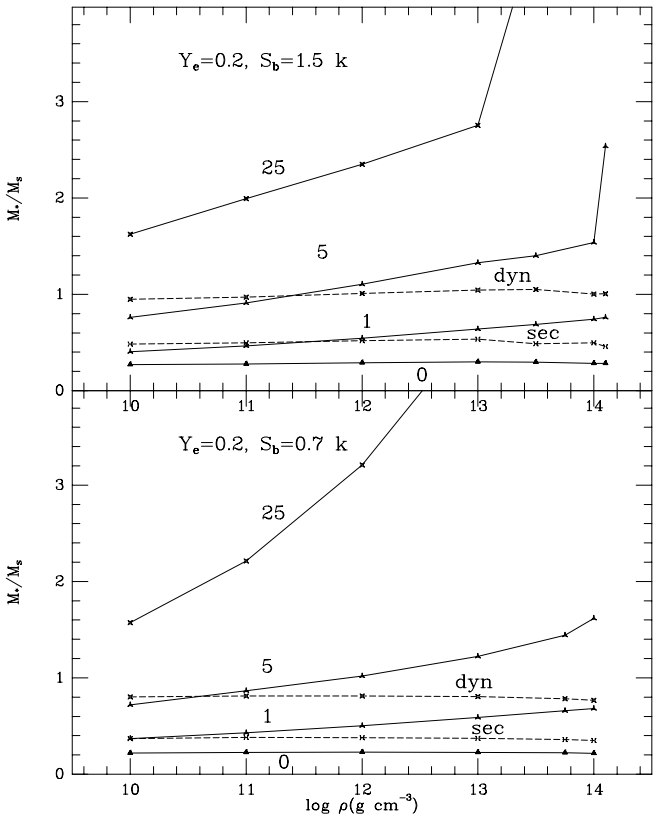

FIG. 2b

FIG. 2.—M_c-ρ_c relations for rotating objects computed for $K = 180$ MeV, $Y_e = 0.2$ and 0.3, and $S_b = 0.7k$ and $1.5k$. The $Y_e = 0.3$ results are shown in Fig. 2*a*, and the $Y_e = 0.2$ results are shown in Fig. 2*b*. The solid lines are for $J = 0$ ("0"), 10^{49} g cm^2 s^{-1} ("1"), 5×10^{49} g cm^2 s^{-1} ("5"), and 2.5×10^{50} g cm^2 s^{-1} ("25"). The dotted lines are for the bar mode secular (sec) and the bar mode dynamic (dyn) stability limits.

$\dot{J}_{\rm GW} = -6.30 \times 10^{47}$ g cm^2 s^{-2}, roughly 3 orders of magnitude smaller than the Newtonian torque. For the $\rho_c > \rho_{\rm nuc}$ fizzler, $M_b = 2.18\ M_\odot = 0.85M$, $J_b = 5.28 \times 10^{49}$ g cm^2 $s^{-1} = 0.69J$, and $R_b = 28$ km $= 0.43\ R_{\rm eq}$. The Newtonian torque $\dot{J}_b = -3.11 \times 10^{51}$ g cm^2 s^{-2}, and the GRR torque $\dot{J}_{\rm GW} = -5.35 \times 10^{49}$ g cm^2 s^{-2}. Although $\dot{J}_{\rm GW}$ is still $\ll \dot{J}_b$, it is considerably enhanced relative to $\dot{J}_b$ for the $\rho_c > \rho_{\rm nuc}$ fizzler. Some of the increased relative importance of gravitational radiation is due to the smaller mass fraction of the spiral arms, but most of it is due to the fact that the higher density of the second model puts it further into the relativistic regime.

4. DISCUSSION: FIZZLER EVOLUTION

4.1. *Rotating Precollapse Cores*

The iron cores of massive stars have $M_{\rm core}$ in the range 1.25–2.05 $M_\odot$ (Timmes et al. 1996) and $Y_e \sim 0.4$–0.49 and $S_b/k \sim 1$–2 (see Hashimoto 1995). As argued by Hayashi et al. (1998, 1999) and corroborated by our own calculations, if a core has angular momentum $J_{\rm core} \gtrsim 10^{49}$ g cm^2 s^{-1}, its collapse is likely to fizzle and avoid a supernova outburst (see also Zwerger & Müller 1997). For comparison, note that the fastest *normal* pulsar PSR J0537−6910 (Marshall et al. 1998) has spin period 16 ms, which, for neutron star parameters, implies $J_{\rm PSR} \sim 10^{48}$ g cm^2 s^{-1}. The fastest *millisecond* pulsars have $J_{\rm PSR} \sim 10^{49}$ g cm^2 s^{-1}. The fact that the most rapidly spinning pulsars are near the fizzler J-threshold suggests that rotation plays an important role in their formation. However, for the millisecond pulsars, it is also possible that their rapid spin is due to the accretion of mass and angular momentum from a companion star. Recent work on the quasi-periodic oscillations of soft X-ray transients implies that two systems contain nearly maximally rotating black holes (Cui, Zhang, & Chen 1998). The system for which the most information is available (GRO J1655−40) consists of a 7 $M_\odot$ black hole with a low-mass stellar companion. The black hole angular momentum cannot have been acquired by accretion through mass transfer because the companion mass is too low. It seems that rotation must have played a role in the collapse that produced this black hole. Further, observations of the most rapidly rotating upper main-sequence stars suggest that their central regions could have $J_{\rm core}$ as large as 10^{50} g cm^2 s^{-1} (Hayashi et al. 1998), well within the regime of interesting fizzler phenomena (see Fig. 2).

Prefizzler cores do not spin rapidly in a dynamical sense, even for the large $J_{\rm core}$ required for fizzler formation. For example, white dwarf models with $M \sim 1.3\ M_\odot$ and $n' = 0$ have $T/|W| \lesssim 0.01$ for $J = 10^{49}$ g cm^2 s^{-1} and $T/|W| \lesssim 0.07$ for $J = 10^{50}$ g cm^2 s^{-1}. Precollapse cores are thus supported primarily by relativistically degenerate electrons, not rotation. Because radiation pressure, electrostatic effects, hot iron nuclei, and the nonzero surface pressure of the core are not negligible, white dwarfs or pure nonrotating $n = 3$ polytropes serve only as guides to the structures of the cores. It is clear, however, that the precollapse cores will be strongly centrally condensed, and so $n' = 0$ is probably not an appropriate choice for $h(m_c)$. If the precollapse core is in uniform rotation, we expect the fizzler that

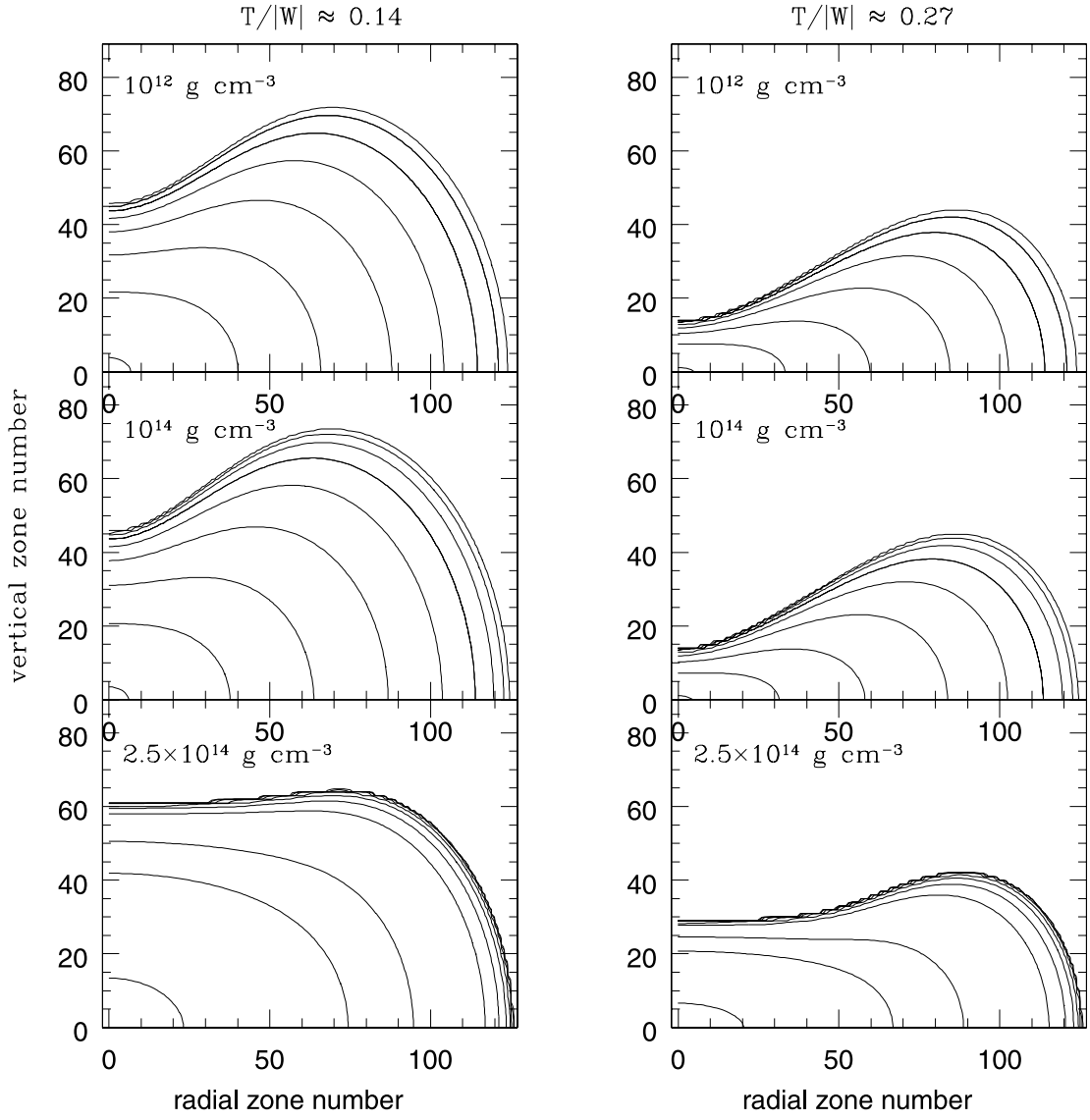

FIG. 3.—Comparison of the equilibrium structures for fizzlers calculated with $n' = 0$ and EOS parameters $Y_e = 0.2$, $S_b = 1.5k$, and $K = 180$ MeV. The left-hand panels are for $T/|W| \approx 0.14$, and the right-hand panels are for $T/|W| \approx 0.27$, the approximate secular stability and dynamic stability limits. The top row of models is for $\rho_c = 10^{12}$ g cm^{-3}. The middle row of models is for $\rho_c = 10^{14}$ g cm^{-3}. The bottom row of models is for $\rho_c = 2.51 \times 10^{14}$ g cm^{-3}. The contour levels are set to $\rho/\rho_c = 0.9$, 0.1, 0.01, 0.001, 10^{-4}, 10^{-5}, 10^{-6}, and 10^{-7}. For $T/|W| \approx 0.14$, the models have mass $M = 0.520$, 0.497, and 1.24 $M_\odot$; and $J = 8.66 \times 10^{48}$, 3.69×10^{48}, and 1.22×10^{49} g cm^2 s^{-1} for $\rho_c = 10^{12}$, 10^{14}, and 2.51×10^{14} g cm^{-3}. For $T/|W| \approx 0.27$, the models have $M = 1.12$, 1.07, and 2.61 $M_\odot$; and $J = 5.11 \times 10^{49}$, 2.20×10^{49}, and 6.71×10^{49} g cm^2 s^{-1} for $\rho_c = 10^{12}$, 10^{14}, and 2.51×10^{14} g cm^{-3}.

forms during the prompt initial collapse of the relatively uniform inner core to have an $h(m_c)$ resembling $n' = 0$. However, as the outer core and inner mantle accrete onto the central core, the overall $h(m_c)$ should become more like $n' = 3$.

The value of n' strongly affects the secular stability limits. However, we argue later that secular instability does not play a large role in early fizzler evolution and so this does not change most of our conclusions. The dynamic stability limit does not depend on n' for $n' \leq 1.5$ (Toman et al. 1998); but, at present, we have little reliable information about the dynamic stability properties of $n' \gtrsim 2$ stellar models for any EOS. The dynamic stability limit may drop as n' increases (Pickett et al. 1996). This would affect our quantitative conclusions; but, for the rest of this discussion, we assume that $n' = 0$ models demonstrate the qualitatively correct fizzler evolutionary behavior.

4.2. *Rotating Core Collapse*

The collapse of rotating stellar cores has been investigated by Zwerger & Müller (1997) and Rampp, Müller, & Ruffert (1998). They showed that the outcome of rotating core collapse depends on the angular velocity distribution, the angular momentum, and effective polytropic index of the collapsing core. However, rotating core collapse is similar to the nonrotating case. The collapse is again nonhomologous; the inner core (the central 0.6–0.8 $M_\odot$ for a typical core) collapses first, while the outer core, to first approximation, remains stationary. The inner core collapses until it either compresses to $\rho_{\rm nuc}$ or becomes centrifugally supported, whereupon collapse halts and the core rebounds to an equilibrium configuration determined by its M and J. This rebound occurs without significant development of nonaxisymmetric structure even if the configuration

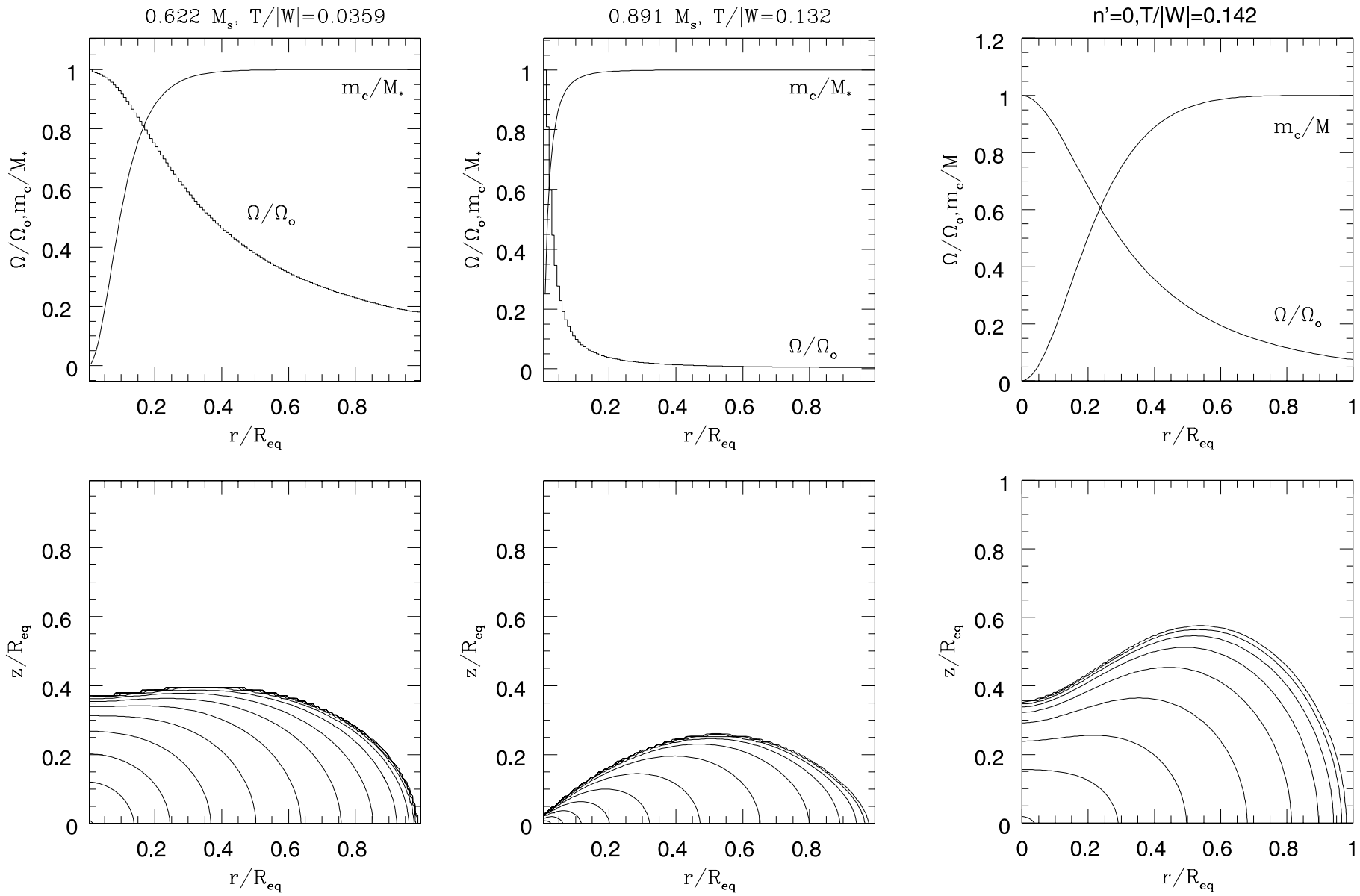

FIG.4*a*

FIG. 4*b*

FIG. 4.—(*a*) Comparison of the equilibrium structures for two $\rho_c = 10^{14}$ g cm^{-3} fizzlers calculated for $n' = 3$ and EOS parameters $Y_e = 0.3$, $S_b = 1.5k$, and $K = 180$ MeV. The left-hand panels are for $T/|W| \approx 0.0359$, and the right-hand panels are for $T/|W| \approx 0.132$. The lower $T/|W|$ model has $M = 0.622\,M_\odot$, and $J = 2.72 \times 10^{48}$ g cm^2 s^{-1}, and the higher $T/|W|$ fizzler has $M = 0.859\,M_\odot$ and $J = 1.41 \times 10^{49}$ g cm^2 s^{-1}. The $T/|W| = 0.0359$ fizzler has central $\Omega_o = 940R$ s^{-1}, and the $T/|W| = 0.132$ fizzler has central $\Omega_o = 2{,}350R$ s^{-1}. In the density plot, the contour levels are set to $\rho/\rho_c = 0.9$, 0.1, 0.01, 0.001, 10^{-4}, 10^{-5}, 10^{-6}, and 10^{-7}. (*b*) The equilibrium structure for a $\rho_c = 10^{14}$ g cm^{-3} fizzler calculated for $n' = 0$ and EOS parameters $Y_e = 0.3$, $S_b = 1.5k$, and $K = 180$ MeV. The fizzler has $T/|W| \approx 0.142$ and central $\Omega_o = 2{,}610R$ s^{-1}. In the density plot, the contour levels are set to $\rho/\rho_c = 0.9, 0.1, 0.01, 0.001, 10^{-4}, 10^{-5}, 10^{-6}$, and 10^{-7}.

TABLE 4

BARLIKE MODE PROPERTIES: $Y_e = 0.3$, $S_b = 1.5k$, $n' = 0$

$T/\|W\|$	M_b ($M_\odot$)	M_d ($M_\odot$)	R_b (km)	J_b (g cm^{2}s^{-1})	τ_b (ms)	τ_{GW} (s)
			$\rho = 10^{12}$ g cm^{-3}			
0.270....	...	...	...	...	...	...
0.284....	2.02	0.60	232	1.22×10^{50}	246	3,580
0.299....	2.14	0.86	235	1.39×10^{50}	194	2,740
0.315....	2.32	1.19	229	1.66×10^{50}	164	2,257
0.323....	2.41	1.40	227	1.83×10^{50}	153	1,910
			$\rho = 10^{13}$ g cm^{-3}			
0.270....	...	...	...	...	...	...
0.284....	1.94	0.61	106	7.98×10^{50}	77.6	180
0.299....	2.18	0.74	104	8.88×10^{50}	62.1	141
0.315....	2.23	1.16	105	1.06×10^{50}	52.9	117
0.324....	2.35	1.46	107	1.26×10^{50}	49.2	107
			$\rho = 10^{14}$ g cm^{-3}			
0.266....	...	...	...	...	...	...
0.280....	1.78	0.52	50.4	4.71×10^{49}	27.9	11.9
0.295....	1.86	0.77	48.2	5.17×10^{49}	22.1	9.15
0.312....	1.95	1.11	47.5	6.01×10^{49}	18.2	7.35
0.329....	2.12	1.58	48.5	48.5×10^{49}	15.6	6.10

TABLE 5

BARLIKE MODE PROPERTIES: $Y_e = 0.2$, $S_b = 1.5k$, $n' = 0$

$T/\|W\|$	M_b ($M_\odot$)	M_d ($M_\odot$)	R_b (km)	J_b (g cm^{2}s^{-1})	τ_b (ms)	τ_{GW} (s)
			$\rho = 10^{12}$ g cm^{-3}			
0.272.....	...	...	...	...	...	...
0.293.....	1.02	0.32	180	4.00×10^{49}	201	9,130
0.330.....	1.23	0.71	184	5.98×10^{49}	143	6,090
0.340.....	1.31	0.86	184	6.74×10^{49}	134	5,640
			$\rho = 10^{13}$ g cm^{-3}			
0.272.....	...	...	...	...	...	...
0.292.....	1.02	0.36	85	2.85×10^{49}	74	495
0.322.....	1.20	0.65	87	3.48×10^{49}	48.0	307
0.330.....	1.26	0.75	86	4.17×10^{49}	45.6	288
			$\rho = 10^{14}$ g cm^{-3}			
0.266.....	...	...	...	...	...	...
0.286.....	0.95	0.32	39.0	1.65×10^{48}	25.0	30.1
0.318.....	1.09	0.62	39.0	2.16×10^{49}	17.1	19.4
0.334.....	1.15	0.89	39.0	2.64×10^{49}	15.3	16.8

reaches large values of $T/|W|$ during the collapse (Rampp et al. 1998). For cores with $J > 10^{49}$ g cm^2 s^{-1}, collapse is halted by the centrifugal barrier at subnuclear densities. During the short time period of collapse and rebound, the Y_e of the inner core material should not decrease dramatically below its initial $Y_e \gtrsim 0.40$, and so it will have $n_{\rm eff} > 3$. According to Zwerger & Müller, an $n_{\rm eff} > 3$ core will settle quickly into equilibrium after its rebound. For $n_{\rm eff} < 3$, they found, instead, that fizzlers execute large amplitude, weakly damped oscillations after rebound. According to the Lattimer & Swesty EOS, oscillations would only be relevant for a significantly deleptonized fizzler ($Y_e \lesssim 0.2$). The equilibrium fizzler produced by the collapse of the low-mass inner core will not have $T/|W| > 0.27$, because, for $Y_e \gtrsim 0.3$, the dynamic stability limit for barlike modes occurs only at fizzler masses $\gtrsim 2\,M_\odot$.

Probably the most important result in Zwerger & Müller is that axisymmetric collapses tend to overshoot the final equilibrium ρ_c and then rebound dynamically. More sophisticated multidimensional calculations will be required to determine whether the shocks generated by the

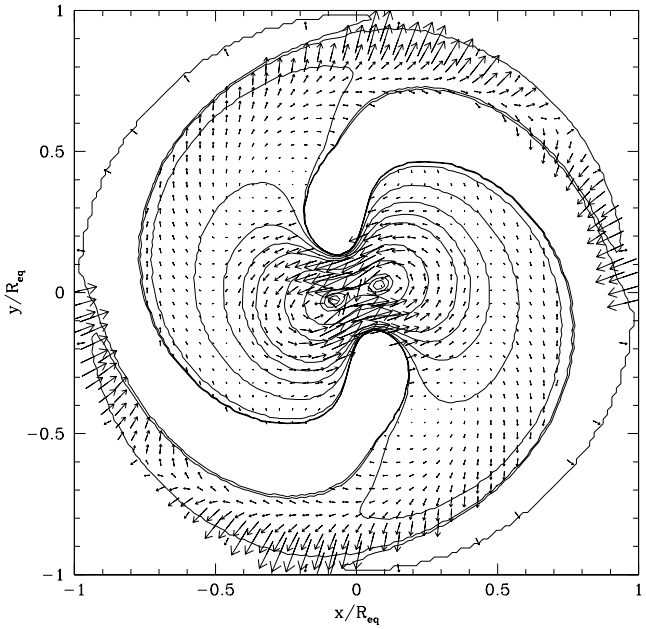

FIG. 5*a*

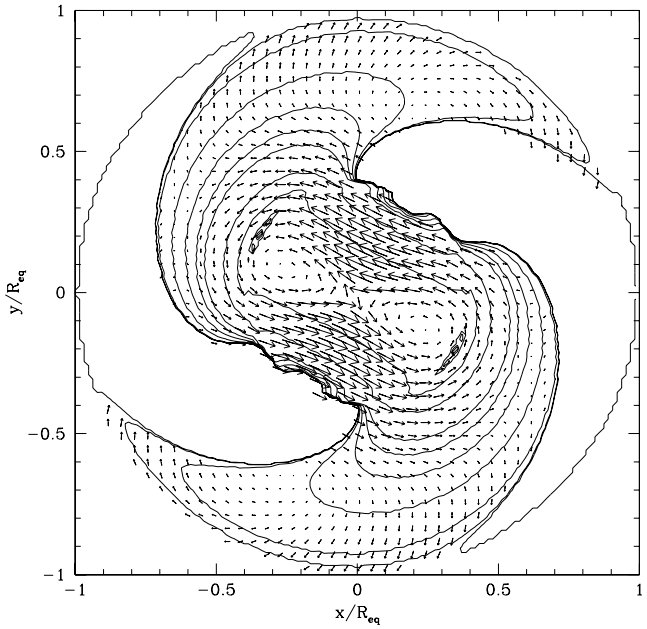

FIG. 5*b*

FIG. 5.—Bar structure for $Y_e = 0.2$ and $S_b = 1.5k$ fizzlers with (*a*) $\rho_c = 10^{14}$ g cm^{-3}, $T/|W| = 0.286$, and initial mass and angular momentum $M = 1.26\,M_\odot$ and $J = 3.13 \times 10^{49}$ g cm^2 s^{-1}; and (*b*) $\rho_c = 2.51 \times 10^{14}$ g cm^{-3}, $T/|W| = 0.303$, and initial mass and angular momentum $M = 2.57\,M_\odot$ and $J = 7.68 \times 10^{49}$ g cm^2 s^{-1}. The eigenfunctions are normalized so that $\delta\mathcal{M} = 1$. The contours are normalized to ρ_c and are for levels 0.0001, 0.001, 0.01, 0.03, 0.06, 0.1, 0.3, 0.6, 0.9, 0.95, 0.98, and 1. The velocity field in the frame of the bar is superimposed on the density contours.

rebound are strong enough to eject some or all of the outer stellar material and perhaps produce a supernova event. In the absence of such calculations, we here consider the likely case that the shocks are not sufficiently strong to prevent the eventual accretion of the outer part of the precollapse core. This should occur on the dynamic timescale of the initial outer core configuration (~ 100 ms for an outer precollapse core with a density $\rho \sim 10^9$ g cm^{-3}).

During accretion, the fizzler may also begin deleptonizing and cooling. For $\rho_c \gtrsim 10^{11}$ g cm^{-3}, neutrinos are trapped in the core and the neutrino diffusion timescale is

$$\tau_{\rm delep} \approx \frac{R_{\rm eq}^2}{c\lambda_{\rm abs}} = (5\text{–}15)\left(\frac{\rho_c}{3 \times 10^{14} g\ {\rm cm}^{-3}}\right) {\rm s}\ , \qquad (19)$$

where $\lambda_{\rm abs}$ is the mean free path for neutrino-nucleon absorption (Prakash et al. 1997). For smaller ρ_c, nucleons are nondegenerate and the coefficient in the $\tau_{\rm delep}$ expression goes from (5–15) to 44. The cooling time for fizzler matter is longer than but comparable to $\tau_{\rm delep}$ (Burrows, Mazurek, & Lattimer 1981). For $M = 1$–$2\ M_\odot$ fizzlers with ρ_c between 10^{12} and 10^{14} g cm^{-3}, $\tau_{\rm delep} \sim 0.15$–5 s, and we expect that deleptonization and cooling effects will not be important during accretion of the outer core except, perhaps, for very low ρ_c fizzlers (large angular momentum cores).

4.3. *Dominance of Dynamic Instability*

We have just argued that the EOS is not likely to change significantly during the inner core collapse and the accretion of the outer core onto the inner core. So, because $Y_e \gtrsim 0.4$, the dynamic barlike instability does not play a role until after accretion because the mass stability limit lies well above 2 $M_\odot$, outside the range of plausible $M_{\rm core}$-values. On the other hand, the secular barlike stability limit falls at $M \sim 1.6$–$1.7\ M_\odot$. So, exceptionally massive fizzlers may be susceptible to secular instability during accretion. Whether this is important or not depends on $\tau_{\rm GRR}$. In Figure 6 we plot $\tau_{\rm GRR}$ for fizzlers with $Y_e = 0.2$ and 0.3 and $S_b = 1.5k$ for $\rho_c = 10^{14}$, 3.16×10^{14}, and 3.98×10^{14} g cm^{-3}. For $\rho_c \lesssim 10^{14}$ g cm^{-3}, $\tau_{\rm GRR}$ is typically $\gtrsim 100$ s; and it is $\gg 100$ s for much lower ρ_c (see Tables 1 and 2). We conclude that, for $\rho_c \lesssim \rho_{\rm nuc}$, the entire outer core will accrete before secular instability has time to set in for any Y_e (see also Rampp et al. 1998). Only if $\rho_c \gtrsim \rho_{\rm nuc}$ can $\tau_{\rm GRR}$ be small enough to allow secular instabilities to grow. We would then be dealing with direct formation of a rapidly rotating, hot, leptonized proto-neutron star, not a fizzler, however. Further, fizzlers with ρ_c–$\rho_{\rm nuc}$ will have $kT \sim 5$–10 MeV, and viscosity is very efficient and will likely damp GRR-driven secular instabilities (Ipser & Lindblom 1991). So, not only is the EOS unlikely to change much during accretion of the outer core, but the high Y_e and long $\tau_{\rm GRR}$ mean that no nonaxisymmetric instabilities will have time to grow.

In preceding sections, when constructing equilibrium models for rotational stability analyses, we assumed that there were zero surface stresses—in other words, that shocks and accretion effects were negligible. The arguments in the paragraph above show that, in fact, significant secular or dynamic instabilities are not likely to occur before the accretion phase is over. Models with zero surface boundary conditions should be adequate for that purpose. In a similar investigation of interstellar cloud collapse (Imamura et al. 2000), we also found that conclusions based on zero surface

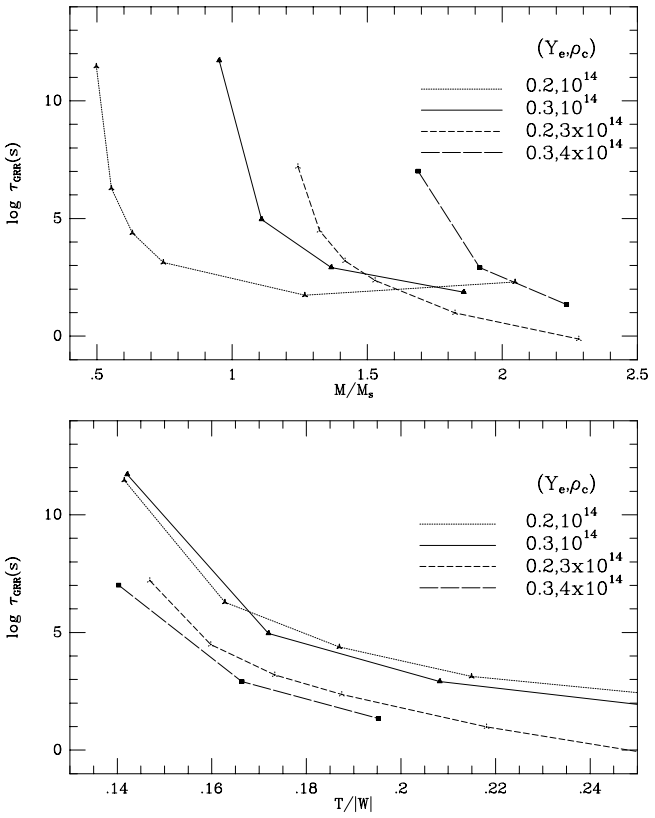

FIG. 6.—Secular instability growth time $\tau_{\rm GRR}$ for fizzlers with $Y_e = 0.2$ and 0.3, and $S_b = 1.5k$. The curves in each panel are for fizzlers with $(Y_e, \rho_c) = (0.2,10^{14})$ (*dotted line*), $(0.3,10^{14})$ (*solid line*), $(0.2, 3.16 \times 10^{14}$ (*short-dashed line*), and $(0.3,3.98 \times 10^{14})$ (*long-dashed line*) g cm^{-3}. The ρ_c are chosen to straddle the line $\rho_c = \rho_{\rm nuc}$. The trial functions used in the evaluation of $\tau_{\rm GRR}$ are determined as described in § 2.3.

boundary condition models agreed reasonably well, both quantitatively and qualitatively, with three-dimensional collapse simulations by Bate (1998). So, in our further discussion, we ignore the accretion phase and assume that a hot, lepton-rich equilibrium fizzler forms which contains all of the initial $M_{\rm core}$. We further assume that our models represent the structure of this core with reasonable accuracy within the constraints of our simplified EOS.

After accretion, the inner region of the equilibrium fizzler has $Y_e \sim 0.4$ and $S_b/k \sim 1$, and the hot accreted envelope has $Y_e \sim 0.4$ and $S_b/k \sim 4$–5 (see Strobel et al. 2000). The further evolution is then driven by decreases in S_b (cooling) and Y_e (deleptonization). There are two main consequences: (1) Study of Figure 2 and Tables 1 and 2 shows that a fizzler that cools and deleptonizes at fixed M and J must contract to higher ρ_c. This is manifested in Figure 2 by the drop in M of the curves of constant J as Y_e and S_b decrease. (2) For fixed Y_e and S_b, the secular and dynamic stability limits for the barlike modes are nearly constant in mass over fizzler densities. For $Y_e \lesssim 0.3$, the dynamic barlike stability limit drops below 2 $M_\odot$. A dynamically unstable bar mode will organize itself out of low-amplitude random noise with an e-folding time given by τ_g in Tables 1 and 2 (see Imamura et al. 2000). The τ_g are in the range of a few to several tens of milliseconds. Although it might take tens of e-folds for the mode to reach nonlinear amplitude, this would still be a shorter time than $\tau_{\rm delep}$. The dynamic barlike instability should thus have time to grow even if there are not large

nonaxisymmetric seed perturbations from the collapse. The only way this fate can be avoided is if deleptonization and cooling cause the fizzler to reach $\rho_c \gtrsim \rho_{\rm nuc}$ before dynamic instability. The mass stability limit rises abruptly at nuclear density.

So, contrary to traditional thinking, in which the secular barlike instability is the first to occur and gently evolves the object toward neutron star densities (e.g., Hayashi et al. 1998), we find that cooling and deleptonization always cause a fizzler to encounter and manifest dynamic barlike instabilities, as long as the fizzler does not reach nuclear densities first. Secular effects cannot trigger barlike instabilities in fizzlers simply because they do not have time to grow. It is thus essential to understand how the dynamically unstable barlike modes behave in fizzlers.

4.4. *Dynamic Bar Mode Growth*

Consider the case in which the dynamic barlike instability has occurred while still at fizzler densities. When the bar mode instability reaches nonlinear amplitude, the Newtonian self-interaction torques transport angular momentum from the bar to the spiral arms. The bar mode saturates at peak amplitude when the time required to drive $J_b \rightarrow J_{\rm dyn}(M_b)$ becomes comparable to τ_g (Imamura et al. 2000). Here $J_{\rm dyn}(M_b)$ is the J of the axisymmetric state with mass M_b that is marginally dynamically stable to barlike modes. After saturation, the evolution remains dynamic for several τ_g. As the bar sheds angular momentum to the outer spiral arms, it should compress rapidly because of the softness of the fizzler EOS and may separate physically from the surrounding spiral arms (see protostellar collapses by Bate 1998 and the $n = 5/2$ calculations in Imamura et al. 2000). If so, the central bar of the fizzler might achieve nuclear densities on a dynamic timescale. If this does not occur immediately, the angular momentum evolution will slow but not stop because the fizzler, although dynamically stable, is still secularly unstable. The slow drain of J from the bar caused by the Newtonian torque and/or by GW emission from the bar itself should maintain the bar amplitude (Imamura et al. 2000; Shibata et al. 2000). The bar evolution should continue until J_b reaches $J_{\rm sec}(M_b)$ or ρ_c reaches $\rho_{\rm nuc}$, whichever comes first. In either case, the fizzler will relax to an axisymmetric state halting its evolution.

A serious complication to any simple scenario building is that the EOS also continues to evolve on the timescale $\tau_{\rm delep}$. If the dynamic stability limit drops below M_b before the bar reaches $\rho_{\rm nuc}$, a second episode of dynamic behavior could ensue. Even without EOS complications, the long-term evolution of bars and even the approach to dynamic instability is still poorly understood (Durisen et al. 2000; Tohline & Durisen 2001).

The fizzler does not radiate significant GW radiation during the early dynamic phase of the evolution; the evolution is driven initially by the Newtonian self-interaction torque (see also Shibata et al. 2000). It is only after J_b drops below $J_{\rm dyn}(M_b)$ that the bar can produce significant GW radiation. We generally expect that the maximum amount of angular momentum fizzlers can radiate is $\Delta J = J_{\rm dyn}(M_b) - J_{\rm sec}(M_b)$ in GW, regardless of the initial $J_{\rm core}$. By fits to our detailed model calculations, we obtain

$$J_{\rm dyn}(M) \sim 1.7\left(\frac{M}{M_\odot}\right)^{1.4} \times 10^{49}\ {\rm g\ cm^2\ s^{-1}} \qquad (20)$$

and

$$J_{\rm sec}(M) \sim 8.6\left(\frac{M}{M_\odot}\right)^{1.4} \times 10^{48}\ {\rm g\ cm^2\ s^{-1}} \qquad (21)$$

for $\rho_c > \rho_{\rm nuc}$. The radiated energy is then

$$\frac{\Delta E}{M_b c^2} \leq \frac{J_{\rm dyn}(M_b)\Omega_p}{M_b c^2} \approx 3 \times 10^{-3}\left(\frac{M_b}{M_\odot}\right)^{0.4}\left(\frac{P_p}{10\ {\rm ms}}\right)^{-1}, \qquad (22)$$

where Ω_p and P_p are the bar mode pattern frequency and period for the marginally stable state.

The bars we have been discussing have M_b-values that are less than any plausible nonrotating neutron star upper mass limit. For $M_{\rm core} < 2\ M_\odot$, M_b is less than $1.3\ M_\odot$, which is less than the measured mass of the binary pulsar (Taylor & Weisberg 1989). The central bar region will thus not collapse to a black hole. This is not the end of the story, however, because the final mass and angular momentum of the neutron star that may form is likely to be greater than M_b and $J_{\rm sec}(M_b)$. Much of the mass shed to the spiral arms may eventually accrete back onto the bar. So the ultimate outcome of the fizzler evolution depends to a great extent on the evolution of the ejected material. This again requires reliable long-term hydrodynamics simulations that include cooling, deleptonization, dissipative heating by shocks, and a realistic EOS. Further, after the fizzler settles into an axisymmetric shape at $J_{\rm sec}(M_b)$ and neutron star densities, it is possible that GRR-driven r-modes could cause further angular momentum loss on a timescale of roughly 1 yr (see Lindblom, Owen, & Morsink 1998).

4.5. *Published Nonlinear Bar Mode Simulations and Gravitational Radiation*

The gravitational radiation produced by $n = 0.5$–1.5 polytropes unstable to the dynamic bar mode instability, has been investigated by several groups in the Newtonian limit (Houser, Centrella, & Smith 1994; Smith et al. 1996; Houser 1998; Rampp et al. 1998; New, Centrella, & Tohline 2000) and by Shibata et al. (2000) in the relativistic limit. Shibata et al. also found that the bar mode dynamic stability limit drops in the relativistic regime to $T/|W| \approx 0.25$, an effect similar to the decrease of the secular barlike stability limit found by Stergioulas & Friedman (1998) in the relativistic regime. Long-term hydrodynamics simulations that started from axisymmetric equilibria with $T/|W| > 0.27$ were used to determine the GW signature of unstable polytropes in the Newtonian limit; Shibata et al. followed the relativistic bar mode evolution to slightly beyond saturation. Only one investigation of which we are aware has investigated nonaxisymmetric dynamic instabilities in collapsing cores (Rampp et al. 1998).

The efficiency of GW production from bar unstable polytropes can be high but depends strongly on the final properties of the central object. As first described by Durisen et al. (1986), the early nonlinear outcome of all unstable barlike mode simulations is the same: the formation of a dynamically stable central bar that resembles a Dedekind-like Riemann S-type ellipsoid surrounded by expanding spiral arms. However, after the early nonlinear phase of evolution, the predictions of the simulations diverge. Some lead to axisymmetric central objects surrounded by disks, while others lead to long lived central bars. According to Houser (1998), to within a factor of order unity, GW energies as

large as

$$\frac{\Delta E}{Mc^2} \approx \left(\frac{GM}{R_{\rm eq}c^2}\right)^{7/2} \tag{23}$$

can be produced by $n = 0.5$ polytropes if long-lived bars form. For 1.4 $M_\odot$ polytropes with $R_{\rm eq} = 15$ and 50 km, $\Delta E/(Mc^2) \sim 0.002$ and 10^{-6}.

The long-term evolution appears to depend as sensitively on numerical techniques as on real hydrodynamic and thermal effects (Tohline, Durisen, & McCollough 1985; Williams & Tohline 1987, 1988; Pickett et al. 1996; Toman et al. 1998; Imamura et al. 2000; New et al. 2000; Durisen et al. 2000, Tohline & Durisen 2001). This is an issue that needs to be addressed with considerable care before the observable properties of fizzlers can be accurately predicted.

5. SUMMARY

The stability properties of fizzlers are similar to those of Maclaurin spheroids and polytropes. For fizzlers with angular momentum distributions $h(m_c)$ similar to that of the Maclaurin spheroids ($n' = 0$), the secular instability and dynamic instabilities of barlike modes set in for $T/|W| \gtrsim 0.14$ and 0.27, respectively, the same limits as found for the Maclaurin spheroids. On the other hand, for fizzlers with angular momentum distributions that concentrate more J toward the equatorial radius than does the Maclaurin spheroid $h(m_c)$, the secular stability limits drop significantly. For the most extreme case we consider ($n' = 3$), one which should be a good approximation for a precollapse iron core in uniform rotation, the bar mode secular stability limit drops to $T/|W| \approx 0.038$. This sense of change is the same as found by Imamura et al. (1995) for polytropes, but the effect here is more extreme. The bar mode dynamic stability limit does not appear to depend strongly on n' for values up to 1.5, but we could not verify this for all n' because we are unable to generate $n' \gtrsim 2$ equilibrium fizzler models with large enough $T/|W|$.

We have shown that the dynamic barlike mode instability is likely to be much more important for fizzler evolution than the secular one. The dynamic barlike evolution for fizzlers with $\rho_c < \rho_{\rm nuc}$ is driven by the Newtonian gravitational self-interaction torque, not by gravitational radiation reaction. Loss of angular momentum by the central bar as a result of these torques, combined with the soft EOS and further deleptonizaton, could cause rapid collapse or contraction of the central bar to neutron star densities. After nuclear densities are reached and dynamic evolution ceases, GW emission may dominate. The efficiency of GW production depends strongly upon the detailed structure and evolution of the bar and of the ejected spiral arms. If the arms wrap into a nearly axisymmetric disk, the Newtonian coupling between the bar and disk may weaken, and the relative overall importance of GW emission would be enhanced. The ejected arms may instead partially recollapse onto the central bar and produce shocks. The long-term evolution of the bar and surrounding material thus depends sensitively on a variety of factors. Long and accurate hydrodynamics simulations of dynamically unstable objects that include effects of cooling, deleptonization, shock heating, and a realistic EOS may be critical for predicting the correct GW signature and integrated GW luminosity of fizzlers.

The traditional fizzler scenario, namely, collapse to a central density intermediate between white dwarf and neutron star densities followed by a quasi-static approach to neutron star density as a result of GRR-driven secular instability, probably does not occur. For fixed EOS parameters, the stability limits in the fizzler density regime tend to be constant in mass. The limiting masses decrease as the fizzler cools and deleptonizes. For initially large values of the lepton fraction $Y_e(\gtrsim 0.3)$, fizzlers are stable to the dynamic bar mode instability, but cooling and deleptonization drive the dynamic stability mass limit downward in M on a timescale shorter than the GRR timescale for secular instability. Fizzlers thus become dynamically unstable to the barlike modes before secular instabilities can grow appreciably.

J. I. thanks the National Aeronautics and Space Administration for support. R. D. enjoyed the hospitality of the Max Planck Institute for Extraterrestrial Physics as a Humboldt Awardee during part of this research.

APPENDIX

LINEARIZED EVOLUTION EQUATIONS

The evolution equations form a set of partial differential equations that describes the time evolution of infinitesimal perturbations about equilibrium. The evolution equations are complex and solved by converting each complex equation to a pair of real equations. The set of real linearized evolution equations is

$$\frac{\partial \eta_R}{\partial t} = m\Omega\eta_I - T_R\left(\frac{\rho_o}{\varpi}\right)\left(1 + \frac{\partial \ln \rho_o}{\partial \ln \varpi}\right) - W_R\frac{\partial \rho_o}{\partial z} - \rho_o\left[\frac{\partial T_R}{\partial \varpi} - \left(\frac{m}{\varpi}\right)V_I + \frac{\partial W_R}{\partial z}\right], \tag{A1}$$

$$\frac{\partial \eta_I}{\partial t} = -m\Omega\eta_R - T_I\left(\frac{\rho_o}{\varpi}\right)\left(1 + \frac{\partial \ln \rho_o}{\ln \partial \varpi}\right) - W_I\frac{\partial \rho_o}{\partial z} - \rho_o\left[\frac{\partial T_I}{\partial \varpi} + \left(\frac{m}{\varpi}\right)V_R + \frac{\partial W_I}{\partial z}\right], \tag{A2}$$

$$\frac{\partial T_R}{\partial t} = m\Omega T_I + 2\Omega V_R - \left(\frac{1}{\rho_o}\right)\frac{\partial \Pi_R}{\partial \varpi} + \left(\frac{\eta_R}{\rho_o^2}\right)\frac{\partial P_o}{\partial \varpi} - \frac{\partial \Phi_R}{\partial \varpi}, \tag{A3}$$

$$\frac{\partial T_I}{\partial t} = -m\Omega T_R + 2\Omega V_I - \left(\frac{1}{\rho_o}\right)\frac{\partial \Pi_I}{\partial \varpi} + \left(\frac{\eta_I}{\rho_o^2}\right)\frac{\partial P_o}{\partial \varpi} - \frac{\partial \Phi_I}{\partial \varpi}, \tag{A4}$$

$$\frac{\partial V_R}{\partial t} = m\Omega V_I - \left(\frac{T_R}{\varpi}\right)\frac{\partial(\Omega\varpi^2)}{\partial\varpi} + \left(\frac{m}{\varpi}\right)\left[\left(\frac{1}{\rho_o}\right)\Pi_I + \Phi_I\right], \tag{A5}$$

$$\frac{\partial V_I}{\partial t} = -m\Omega V_R - \left(\frac{T_I}{\varpi}\right)\frac{\partial(\Omega\varpi^2)}{\partial\varpi} - \left(\frac{m}{\varpi}\right)\left[\left(\frac{1}{\rho_o}\right)\Pi_R + \Phi_R\right], \tag{A6}$$

$$\frac{\partial W_R}{\partial t} = m\Omega W_I - \left(\frac{1}{\rho_o}\right)\frac{\partial\Pi_R}{\partial z} + \left(\frac{\eta_R}{\rho_o^2}\right)\frac{\partial P_o}{\partial z} - \frac{\partial\Phi_R}{\partial z}, \tag{A7}$$

$$\frac{\partial W_I}{\partial t} = -m\Omega W_R - \left(\frac{1}{\rho_o}\right)\frac{\partial\Pi_I}{\partial z} + \left(\frac{\eta_I}{\rho_o^2}\right)\frac{\partial P_o}{\partial z} - \frac{\partial\Phi_I}{\partial z}, \tag{A8}$$

where

$$\rho_1 = \eta_R + i\eta_I\,, \qquad P_1 = \Pi_R + i\Pi_I\,, \qquad v_{\varpi,1} = T_R + iT_I\,, \qquad v_{\phi,1} = V_R + iV_I\,, \quad \text{and} \quad v_{z,1} = W_R + iW_I\,. \tag{A9}$$

The gravitational perturbation is found from

$$\nabla^2\Phi_1 = 4\pi G\rho_1\,, \tag{A10}$$

where

$$\Phi_1 = \Phi_R + i\Phi_I\,. \tag{A11}$$

The Φ_R and Φ_I are found separately from η_R and η_I, respectively. The evolution equation set is closed by

$$P_1 = \rho_1\frac{\partial P}{\partial\rho}\Big|_{\rho=\rho_o}\,. \tag{A12}$$

REFERENCES

Abramovici, A., et al. 1995, Particle and Nuclear Astrophysics and Cosmology in the Next Millennium, ed. E. W. Kolb & R. Peccei (Singapore: World Scientiific), 398
Bardeen, J. M., Friedman, J. L., Schutz, B. F., & Sorkin, R. 1977, ApJ, 217, L49
Bate, M. R. 1998, ApJ, 508, L95
Bodenheimer, P., & Ostriker, J. P. 1973, ApJ, 180, 159
Burrows, A., Mazurek, T. J., & Lattimer, J. M. 1981, ApJ, 251, 325
Chandrasekhar, S. 1969, Ellipsoidal Figures of Equilibrium (New Haven: Yale Univ. Press)
Clement, M. J. 1979, ApJ, 230, 230
Cui, W., Zhang, S. N., & Chen, W. 1998, ApJ, 494, L53
Durisen, R. H. 1977, ApJ, 213, 145
Durisen, R. H., Gingold, R. A., Tohline, J. E., & Boss, A. P. 1986, ApJ, 305, 281
Durisen, R. H., Pickett, B. K., Bate, M. R., Imamura, J. N., Brandtl, A., & Sterzik, M. F. 2000, in poster presentations of IAU Symp. 200, Birth and Evolution of Binary Stars, ed. B. Reipurth & H. Zinnecker (Potsdam: Astrophysikalisches Institut), 187
Eriguchi, Y., & Müller, E. 1991, A&A, 248, 435
Finn, L. S., & Evans, C. R. 1990, ApJ, 351, 588
Friedman, J. L., & Schutz, B. F. 1978, ApJ, 222, 281
Gold, T. 1974, in Seventh Texas Symp. on Relativistic Astrophysics, ed. P. G. Bergmann, E. J. Fenres, & L. Motz (New York: NY Acad. Sci.)
Hachisu, I. 1986, ApJS, 61, 479
Hashimoto, M. 1995, Prog. Theor. Phys., 94, 663
Hayashi, A., Eriguchi, Y., & Hashimoto, M. 1998, ApJ, 492, 286
———. 1999, ApJ, 521, 376
Houser, J. L. 1998, MNRAS, 299, 1069
Houser, J. L., Centrella, J. M., & Smith, S. 1994, Phys. Rev. Lett., 72, 1314
Imamura, J. N., Durisen, R. H., & Pickett, B. K. 2000, ApJ, 528, 946
Imamura, J. N., Toman, J., Durisen, R. H., Pickett, B., K., & Yang, S. 1995, ApJ, 444, 363
Ipser, J., & Lindblom, L. 1991, ApJ, 373, 213
Lattimer, J., & Swesty, D. 1991, Nucl. Phys. A, 535, 331
Lindblom, L., & Detweiler, S. 1977, ApJ, 211, 565
Lindblom, L., Owen, B., & Morsink, S. M. 1998, Phys. Rev. Lett., 80, 4843
Lynden-Bell, D., & Ostriker, J. P. 1967, MNRAS, 136, 293
Marshall, F. E., Gotthelf, E. V., Zhang, W., Middleditch, J., & Wang, Q. D. 1998, ApJ, 499, L79
Müller, E., & Eriguchi, Y. 1985, A&A, 152, 325
New, K. C. B., Centrella, J., & Tohline, J. E. 2000, Phys. Rev. B, submitted
Pickett, B. K., Durisen, R. H., & Davis, G. A. 1996, ApJ, 458, 714
Prakash, M., Bombaci, I., Prakash, M., Ellis, P. J., Lattimer, J. M., & Knorren, R. 1997, Phys. Rep., 280, 1
Rampp, M., Müller, E., & Ruffert, M. 1998, A&A, 332, 969
Shapiro, S. L., & Lightman, A. P. 1976, ApJ, 207, 263
Shapiro, S. L., & Teukolsky, S. A. 1983, Black Holes, White Dwarfs, and Neutron Stars (New York: Wiley)
Shibata, M., Baumgarte, T. W., & Shapiro, S. L. 2000, ApJ, 542, 453
Smith, S. C., Houser, J. L., & Centrella, J. M. 1996, ApJ, 458, 236
Stergioulas, N., & Friedman, J. L. 1998, ApJ, 492, 301
Strobel, K., Schaab, C., & Weigel, M. K. 2000, A&A, submitted
Tassoul, J.-L. 1978, Theory of Rotating Stars (Princeton: Princeton Univ. Press)
Taylor, J. H., & Weisberg, J. M. 1989, ApJ, 345, 434
Timmes, F. X., Woosley, S. E., & Weaver, T. A. 1996, ApJ, 457, 834
Tohline, J. E. 1984, ApJ, 285, 721
Tohline, J. E., & Durisen, R. H. 2001, in The Formation of Binary Stars, ed. H. Zinnecker & R. Mathieu (San Francisco: ASP), in press
Tohline, J. E., Durisen, R. H., & McCollough, M. 1985, ApJ, 298, 220
Toman, J., Imamura, J. N., Pickett, B. K., & Durisen, R. H. 1998, ApJ, 497, 370
Williams, H. A., & Tohline, J. E. 1987, ApJ, 315, 594
———. 1988, ApJ, 334, 449
Zwerger, T., & Müller, E. 1997, A&A, 320, 209